Imaging Metallic Samples Using Electrical Capacitance Tomography: Forward Modelling and Reconstruction Algorithms

E Al Hosani[1], M Zhang[1], J. F. P. J. Abascal[2] and M Soleimani[1]
[1]Engineering Tomography Lab (ETL), Department of Electronic and Electrical Engineering, University of Bath, Bath, UK
[2]CREATIS (CNRS UMR 5220 – INSERM U1206 – Université Lyon 1 – INSA Lyon - Université Jean Monnet Saint-Etienne), Villeurbanne, France
Email: m.soleimani@bath.ac.uk

Abstract: *Electrical Capacitance Tomography (ECT) is an imaging technology used to reconstruct the permittivity distribution within the sensing region. So far ECT was primarly used to image non-conductive media only. This is because if the conductivity of the imaged object is high, the capacitance measuring circuit will be almost shortened by the conductivity path and a clear image cannot be produced using the standard image reconstruction approaches. This paper tackles the problem of imaging metalic samples using conventional ECT systems by investigating the two main aspects of image reconstruction algorithms, namely the forward problem and the inverse problem. For the forward problem, two different methods to model the region of high conductivity in ECT is presented. On the other hand, for the inverse problem, three different algorithms to reconstruct the high contrast images are examined. The first two methods which are linear single step Tikhonov method and iterative Total Variation regularization method use two sets of ECT data to reconstruct the image in time difference mode. The third method, namely Level Set method, uses absulute ECT measurments and was developed using matalic forward model. The results indicate that the applications of conventional ECT systems can be extended to metal samples using the suggested algorithms and forward model, especially using level-set algorithm to find the boundary of the metal.*
Keywords: Electrical Capacitance Tomography, metal sample, high conductivity, forward model, Total Variation, Level Set

1 INTRODUCTION

Electrical Capacitance Tomography (ECT) is a method used for imaging the cross-section of an object. It measures the external capacitance of the bounded object in order to determine the internal permittivity distribution, which is then used to obtain an image of the object's interior. The first ECT system was developed in the 80s [1] and since then it has been constantly enhanced and modified to be adapted in modern applications [2-13]. However, there are some challenges that make image reconstruction using ECT system a challenge such as the soft field effect where the inhomogeneous generated electric field lines in the region of interest tend to spread and become dependent on the physical electrical properties of the material of interest (the permittivity). Thus, no distinct border between the pixels can be obtained. The soft field effect triggers more challenges to ECT such as ill-conditioning in which a small error in the input (capacitance measurements) can result in much larger errors in the solution (permittivity distribution), which leads to unstable solutions. Furthermore, the system is underdetermined as the number of variables in the system model (number of pixels) is greater than the number of equations (number of capacitance measurements). This is because the system hardware is limited to a certain number of electrodes, and thus limited number of independent measurements, which are much less than the number of pixels used to reconstruct the image. In addition, the relationship between the measured capacitance and the permittivity distribution is considered nonlinear. However, a linearized model is often used instead. Furthermore, since the physical properties of an object depend on both permittivity and conductivity, ECT systems are mainly used to image non-conductive media. This is because the conductivity of the material will have a great effect on the capacitance measurement sensor. Only when the

conductivity of the imaged object is very low, its effect on the ECT system can be ignored. However, if the conductivity of the imaged object is high, the capacitance measuring circuit will be almost shortened by the conductivity path and a clear image cannot be produced using the standard image reconstruction approaches. This limitation stands on the way of ECT to be of more use in the process or medical industries as most of the media encountered are conductive. However, ECT systems have other advantages that made this new technology more promising for many industrial applications such as being cost effective, non-hazardous, non-invasive, non-intrusive and fast.

This paper challenges the above-mentioned limitations by attempting to adapt conventional ECT systems to image metallic objects (i.e highly conductive) with high resolution. Different from dielectric specimen whose conductivity is negligibly low, metallic material normally is of high conductivity ($\delta > 10^8$ S/m). Any electric field applied through a conductor will force the inner free charges to move until the net electric field is zero inside the conductor, i.e., the electric potential is the same on any point of the conductor. In ECT, the electrostatic equilibrium on metallic materials will create an increment on the measured capacitances. Therefore, in [14] a new application of ECT on metallic sample imaging is developed. This paper sets out to allow a better understanding of how metallic samples could be imaged using conventional ECT device and how state of the art algorithms could enhance this application. It has been proposed that ECT could potentially monitor liquid metal flow in metallurgy process. From the literature, three reportedly powerful techniques suggested high potential in solving our problem (i.e imaging metallic samples using ECT) namely Total Variation regularization [30] and Level Set method [26] and the most commonly used Tikhonov method.

Total variation regularisation was first introduced by [15] and since then it has been mainly applied to digital image processing for noise removal [15] and to solve the *compressed sensing* problem (aka sparse sensing) in different applications [29]. Total variation assumes that the unknown object is piecewise constant, which allows suppressing noise while maintaining sharp edges in the reconstructed image. Total variation has been also used to regularize the inverse problem in different tomographic applications [22]. The split Bregman formulation has been shown to efficiently solve the constrained total variation problem [22-23].

The level set method was first developed in the 1980s by Osher and Setain for modelling the front propagation of surfaces under curvature [16]. Santosa [17] then was able to adapt the concept of level set to solve inverse problems using two computational approaches. The first approach is based on a nonlinear time-dependent partial differential equation (i.e Hamilton-Jacobi equation). The second approach uses optimization to produce a sequence of level set functions that minimize the residual. Other studies were conducted using different types of level set techniques for electrical and electromagnetic tomographic shape reconstruction [18, 19].

This paper is divided as follows: section 2 introduces and discusses the forward model of the ECT system along with the two suggested forward models for metal imaging. Section 3 introduces the inverse problem solutions. Section 4 shows and compares the experimental results while section 5 gives a discussion about the results.

2 THE FORWARD PROBLEM MODELLING

2.1 Traditional ECT Forward Model

The ECT mathematical system model can be treated as an electrostatic field problem and hence can be modelled by Poisson's equation (a Laplace's equation with no free charge) as follow

$$\boldsymbol{\nabla}.\left(\boldsymbol{\varepsilon}\,(\boldsymbol{x},\boldsymbol{y})\boldsymbol{\varepsilon_o}\,\boldsymbol{\nabla\phi}(\boldsymbol{x},\boldsymbol{y})\right)=\boldsymbol{0} \tag{1}$$

where ε_o is permittivity of the free space and $\varepsilon\,(x,y)$ is the relative permittivity distribution and $\phi(x,y)$ is the 2-dimensional functions of the electrical potential distributions. The problem can be discretised by using the Finite Element Method (FEM), such that the mutual capacitance C_{ij} for n-electrode capacitance system (when electrode i is the source and electrode j is the detector) can be found by

$$\boldsymbol{C_{ij}}=-\frac{\boldsymbol{\varepsilon_o}}{\boldsymbol{V_{ij}}}\int_{\boldsymbol{\Gamma_j}}\boldsymbol{\varepsilon}\,(\boldsymbol{x},\boldsymbol{y})\,\boldsymbol{\nabla\phi^i}(\boldsymbol{x},\boldsymbol{y}).\hat{\boldsymbol{n}}\,\boldsymbol{d\Gamma_j}\qquad \boldsymbol{for}\begin{pmatrix}\boldsymbol{i}=\boldsymbol{1},\ldots,\boldsymbol{N-1}\\ \boldsymbol{j}=\boldsymbol{i+1},\ldots,\boldsymbol{N}\end{pmatrix} \tag{2}$$

where ϕ^i is the electrical potential distribution when electrode i is excited, γ_j is the surface of the receiving electrode and $\hat{n}$ is a unit vector normal to $\boldsymbol{\Gamma_j}$ which is the surface of the receiving electrodes. For a N-electrode ECT system, $M=\frac{N(N-1)}{2}$ independent measurements can be obtained.

2.2 Forward modelling for metal samples

Since a source electrode is energised, the free charges inside the metal start moving by the force of electric field. The metal will reach the electrostatic equilibrium in a very short time (~10^{-19}s [20]), so the physics of electrostatics used in the ECT forward model can cover the features of metal inside the sensor. Within the metal region, the voltage is the same everywhere:

$$\boldsymbol{\phi^p}=\boldsymbol{\phi^q}\qquad for\ p,q\in\omega_{metal} \tag{3}$$

p,q are any two points on the region of metal, ω_{metal}. From equation (2), the measured capacitance is the surface integration of electric displacement of the sensing electrode. The metal performs like a void of electric field/displacement, shortening the distance between the source and detector electrodes, *i.e.*, the capacitance will be increased.

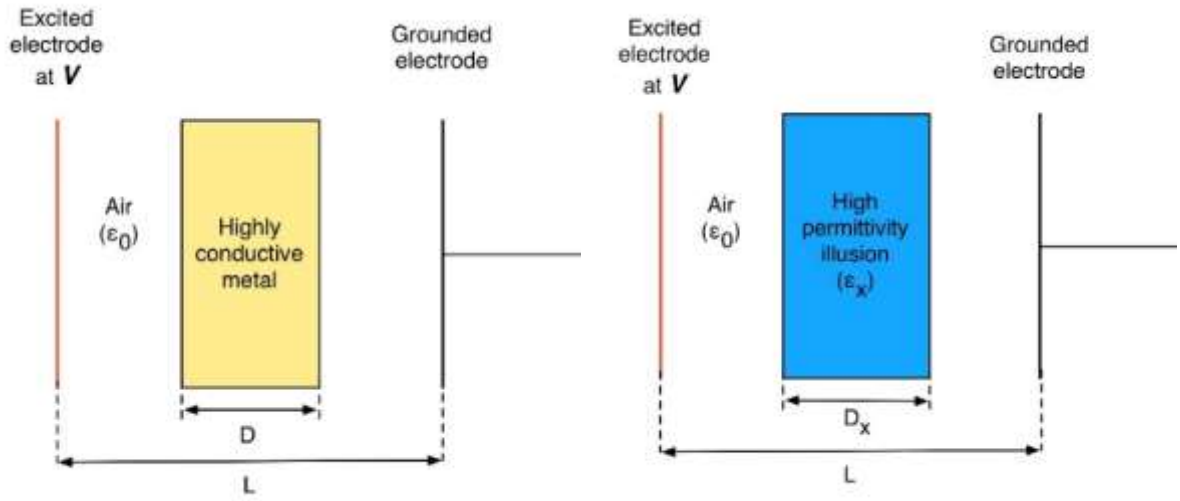

(a) **(b)**

Figure 1. One dimensional analysis of the same capacitances from two different inclusions between a 1d ECT sensor (*i.e.*, a pair of electrodes): (a) a metallic sample of the size D; (b) a dielectric sample of the permittivity of ε_x and size of D_x.

In [14], the authors proposed a 1-dimensional (1D) ECT model (shown in Figure 1) to demonstrate the increase in capacitance by introducing a dielectric illusion of permittivity of $\varepsilon_x = k.\varepsilon_0$, where k is its relative permittivity. To match the capacitance of the metal standing between the two electrodes, the illusion must be of the size of $D_x = \frac{k}{k-1}.D$, where D is the size of the metal [14]. The 1d analysis implies that the metal in ECT can be potentially imaged as a dielectric sample. To make the size of the dielectric illusion close to the metal, $\frac{k}{k-1}$ must be close to 1, *i.e.*,k is a big value. In this paper extends this ECT metallic evaluation model from 1D to 2-dimensional (2D). To validate the implication above, a squared metal of the side length of 0.6 unit length (the external radius of the insulation wall is 1 unit length) is presented as shown in Figure 2.

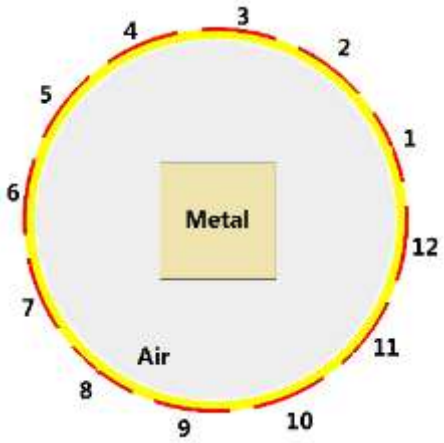

Figure 2. A square metallic sample in a 2D ECT sensor with 12 electrodes.

In first test, *i.e.*, equal potential (EP) model, every point on the region of metal is set as the equal potential which follows the real scenario within the sensor. Then in second test, *i.e.*, high permittivity (HP) model, the metal is replaced by dielectric material: its relative permittivity is set to k =1000, so the dimension is almost the same as the metal, due to $\frac{k}{k-1}$=1.001. The simulation results based on fem is presented in Figure 3

- When electrode 12 is excited, the two sets of electric potential distribution, ϕ_{ep} and ϕ_{hp}, from ep and hp models are plotted in (a) and (c).
- By energising the electrodes in turn, the two sets of 66 mutual capacitances, C_{ep} and C_{hp}, are obtained and plotted as (b) and (d).

In Figure 3(e), the colour bar indicates that the difference between potential distributions of these two models, $\phi_{ep} - \phi_{hp}$ is very small, as the scale of capacitance is modelled as 10^{-11} while the scale of the error is 10^{-16} . this has been clarified. The points of minimum (blue) and maximum (red) electrical potential locate on the two edges of metal facing and far from the energised electrode 12. This shows that the electrical potential on the high permittivity region is decreasing but in very small rate, while it is no potential change on that region in EP model. In Figure 3(f), the difference in the mutual capacitances, $C_{ep} - C_{hp}$ is 5 orders less of magnitude than the C_{ep}, which is at noise level for a real measurement. This means the capacitance measurements cannot tell the difference between the metal and the dielectric of high permittivity of the same size.

ECT imaging is to reconstruct the permittivity distribution within the sensing region, the mutual capacitances is the key input for the process of inverse solver. However, it is not the permittivity of the metallic material under test changes the capacitance measurement, but the electrostatic equilibrium contributes to the change, due to high conductivity. The HP model is approximate model to compensate the zero electric field on that region of metal, meanwhile this approximation convert the problem of imaging metal to dielectric of high permittivity. Therefore, applying the inverse solvers for high contrast problems will result in a promising reconstruction for the metallic material. To bridge the changes in permittivity distribution and the changes in capacitance measurements, a sensitivity matrix, J is built in following equation [21]

$$\boldsymbol{J} = \frac{\partial \boldsymbol{C}_{ij}}{\partial \boldsymbol{\mathcal{E}}(\boldsymbol{x},\boldsymbol{y})} = -\int_{\boldsymbol{\Omega}} \nabla \boldsymbol{\phi}^{\boldsymbol{i}}(\boldsymbol{x},\boldsymbol{y}) \cdot \nabla \boldsymbol{\phi}^{\boldsymbol{j}}(\boldsymbol{x},\boldsymbol{y}) d\boldsymbol{\Omega} \tag{4}$$

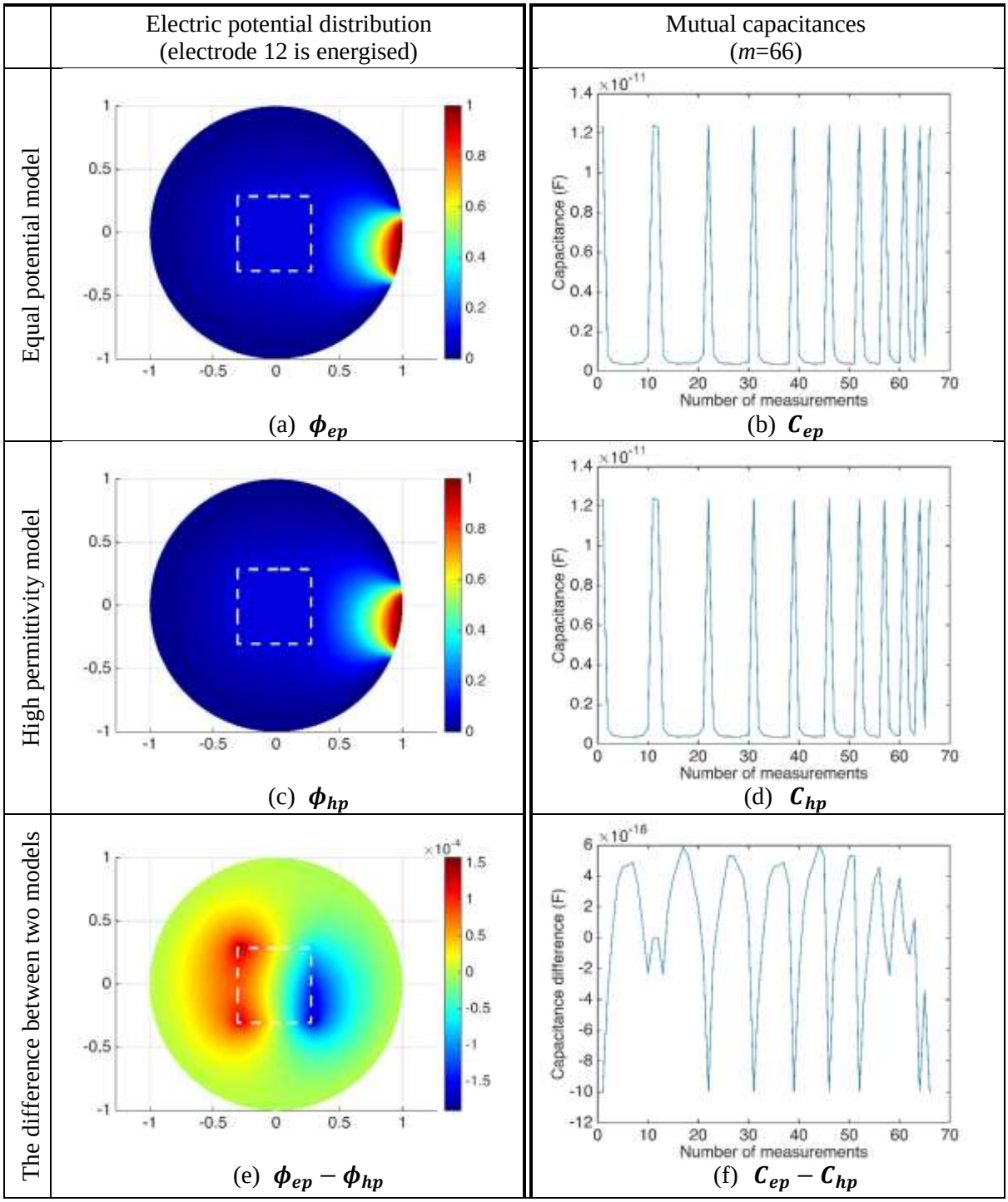

Figure 3. Electric potential distribution of a square metal in ECT (marked by the white dashed lines) and mutual capacitances.

3 THE INVERSION METHODS

3.1 Regularization methods for linear measurements

The image reconstruction in ECT is an inverse problem, which is an ill-posed, ill-conditioned and nonlinear problem. Therefore, approximation methods based on linearization are usually used for ECT to solve the inverse problem. A possible general formulation for the regularized

inverse problem in the form of unconstrained optimization problem is to find the permittivity changes, $\Delta\varepsilon$, to minimize the following function:

$$\|\boldsymbol{J}\Delta\boldsymbol{\varepsilon} - \boldsymbol{m}\|_2^2 + \boldsymbol{\gamma}\boldsymbol{Reg}(\Delta\boldsymbol{\varepsilon}) \quad (5)$$

where $m = C - C_0$, is the capacitance change between measurement of test, C, and a background measurement, C_0, γ is the regularisation factor, and $Reg(\Delta\varepsilon)$ is the stabilizing function commonly selected as

$$\boldsymbol{Reg}(\Delta\boldsymbol{\varepsilon}) = \|\boldsymbol{L_k}(\Delta\boldsymbol{\varepsilon} - \overline{\Delta\boldsymbol{\varepsilon}})\|_{\boldsymbol{n}}^{\boldsymbol{n}} \qquad \infty \geq \boldsymbol{n} \geq \boldsymbol{1} \quad (6)$$

where L_k is the regularisation matrix, which can be any kind of lowpass filters, such as weighted Fourier operator, a derivative operator of order k, a wavelet transform or a finite difference operator of the k[th] derivative in which its dimensions depends on the order of derivative and the boundary conditions. $\Delta\varepsilon$ is the estimated solution of permittivity change from the same reference point.

3.1.1 Tikhonov regularization (single-step linear method)

One of the most commonly used regularization methods for linear ill-posed inverse problems is the Tikhonov regularization, which has been efficiently applied in numerous fields, with satisfactory numerical performances. As mentioned before, if a problem is ill-posed and ill-conditioned, like the sensitivity matrix J, the solution will be non-unique and the computing algorithm will most probably be mathematically unstable, and hence it requires to be regularized before numerical treatment. Tikhonov regularization tries to balance the stability of the solution with its accuracy.

In equation (6) if n=2, and L_k is a finite difference operator with $k \geq 0$, then the regularization is called Tikhonov regularization and is given by

$$\boldsymbol{Reg}(\Delta\boldsymbol{\varepsilon})^{\boldsymbol{TK}} = \|\boldsymbol{L_k}(\Delta\boldsymbol{\varepsilon} - \overline{\Delta\boldsymbol{\varepsilon}})\|_2^2 \quad (7)$$

Consequently, the regularized solution $\widehat{\Delta\varepsilon}$ using tikhonov regularization is found by minimizing the objective functional

$$\boldsymbol{arg}\min_{\Delta\boldsymbol{\epsilon}} \boldsymbol{g}(\Delta\boldsymbol{\varepsilon}) = \|\boldsymbol{J}\Delta\boldsymbol{\varepsilon} - \boldsymbol{m}\|_2^2 + \boldsymbol{\gamma}\,\|\boldsymbol{L_k}(\Delta\boldsymbol{\varepsilon} - \overline{\Delta\boldsymbol{\varepsilon}})\|_2^2 \quad (8)$$

By solving the unconstrained optimization problem (8), an explicit solution, denoted by $\widehat{\Delta\varepsilon}$, is given by:

$$\widehat{\Delta\boldsymbol{\varepsilon}} = (\boldsymbol{J^T J} + \boldsymbol{\gamma}\,\boldsymbol{L^T L})^{-1}\boldsymbol{J^T m} \quad (9)$$

However, it was reported that Tikhonov regularisation does not permit sharp edges when $k > 0$ and only results in smooth edges and oscillations. Therefore, the simplest yet most used form of Tikhonov regularisation is the standard Tikhonov regularisation, which takes $\overline{\Delta\varepsilon} = 0$ in equation (6) and k=0, giving $L_0 = I$, where I is the identity matrix. A Laplacian operator is used for regularization matrix L in this study.

3.1.2 Total Variation (TV) (iterative linear method)

In equation (6) if $\overline{\Delta\varepsilon} = 0$, n=1, and L_k is usually a discrete gradient with $k = 1$, then the regularisation is called total variation regularisation and is given by:

$$Reg(\Delta\varepsilon)^{TV} = \|\nabla(\Delta\varepsilon)\|_1 \tag{10}$$

Equation (10) is equivalent of taking the integral of the absolute gradient of $\Delta\varepsilon$ over the entire sensing domain $\boldsymbol{\Omega}$:

$$\boldsymbol{Reg(\Delta\varepsilon)^{TV}} = \int_{\boldsymbol{\Omega}} |\boldsymbol{\nabla(\Delta\varepsilon)}|\, \boldsymbol{d\Omega} \tag{11}$$

When $\overline{\Delta\varepsilon} = 0$, n=1.

This regularisation technique has advantages over other smoothing techniques such as Tikhonov regularisation, Gaussian smoothing or median filtering, which reduce noise but also smoothen the edges since they cannot reconstruct the jump changes in permittivity at interfaces. By contrast, total variation regularisation removes noise, even in low signal to noise ratios, while keeping important detail such as edges especially when jump changes in permittivity are present. Also, since TV regularisation takes advantage of the sparse structure of the sensitivity matrix, it is considered faster and consumes less amount of memory than standard dense-matrix based algorithms. On the other hand, TV is only capable of restoring functions that are piecewise constant. Moreover, not all underdetermined systems of linear equations have a sparse solution, and therefore total variation cannot be applied for any type of underdetermined linear systems.

There are different varieties for TV algorithms and in this study we use a split bregman TV. Applying the $l_1 - norm$ regularisation method means adding a penalty total variation regularisation term $G_{TV}\ (\Delta\varepsilon)$ to equation (5)

$$\boldsymbol{G_{TV}\ (\Delta\varepsilon)\ = \alpha\|\Delta\varepsilon\|_1} \tag{12}$$

Where α is the regularisation parameter and $\|\cdot\|_1$ is the $l_1 - norm$. The iterative method is based on the bregman distance [15]. For a given convex function $C\ (x)$, the bregman distance between a and b can be defined as

$$D_F\ (a, b) = C\ (a) - C\ (b) - < s, a - b > \tag{13}$$

Where s is the sub gradient of C at b, and $<,>$ denotes the scalar product.
Assuming $\Delta\varepsilon$ is the optimal solution and $\Delta\varepsilon^k$ is the iterative solution, and then minimizing the bregman distance between $\Delta\varepsilon$ and $\Delta\varepsilon^k$ can be used to find the optimal solution. Setting $C\ (x) = R\ (x)$ be the total variation function in this case. The definition of total variation regularisation is as follows: given a differentiable function f defined on a bounded domain $\boldsymbol{\Omega}$, the total variation

$$\boldsymbol{R(f)} = \int_{\boldsymbol{\Omega}} |\boldsymbol{\nabla f\ (x)}|\boldsymbol{dx} = \boldsymbol{\|\nabla f\|_1} \tag{14}$$

Where $\|\nabla f\|_1$ is the $l_1 - norm$ of the gradient of f and can be calculated as the sum of the absolute values over the domain of the function f.
Then the Bregman iterative algorithm can be expressed as following

$$\boldsymbol{\Delta\varepsilon^{k+1} = \mathbf{Min}\, D_R\left(\Delta\varepsilon, \Delta\varepsilon^k\right) + \frac{\lambda}{2}\|J\Delta\varepsilon - m\|^2} \tag{15}$$

Where $\boldsymbol{\lambda}$ is the regularisation parameter. After integrating equation (14) and (15), the sub gradient of the total variation function at the $(k+1)\ th$-iteration

$$s^{k+1} = s^k - \lambda J^T (J\Delta\varepsilon^{k+1} - m) \tag{16}$$

Equation (15) and (16) are the basic formulation of Bregman iterative algorithm and they can be simplified to [11]

$$\Delta\varepsilon^{k+1} = \text{Argmin}\{ R\ (\Delta\varepsilon) + \frac{\lambda}{2} \left\| J\Delta\varepsilon - (m)^k \right\|^2 \} \tag{17}$$

$$(m)^{k+1} = (m)^k + m - J\Delta\varepsilon^{k+1} \tag{18}$$

The Bregman iterative algorithm has several advantages over traditional penalty function. For example, the Bregman iteration converges very quickly when applied to some functions, especially for problems involving $l_1 - norm$. Based on the bregman iterative algorithm, split bregman methods can extend the utility of the bregman iteration to the minimizations of more general $l_1 - norm$ regularisation.

The split Bregman iteration method is introduced as follows: an auxiliary variable d which aims to be optimised to represent ($d = \Delta\varepsilon$) can be used to transfer equation (5) to a constrained optimization problem

$$\boldsymbol{x_\alpha = argmin_{\Delta\varepsilon} \frac{1}{2} \|J\Delta\varepsilon - m\|^2 + \alpha \|d\|_1} \tag{19}$$

To solve this problem, the corresponding unconstrained optimization problem of equation (19)[16] is

$$x_\alpha = argmin_{\Delta\varepsilon} \frac{1}{2} \|J\Delta\varepsilon - m\|^2 + \alpha \|d\|_1 + \frac{\beta}{2} \|d - \Delta\varepsilon\|^2 \tag{20}$$

Where $\beta > 0$ is the split parameter. After applying the bregman iteration method that shown in equation (17) and (18), the solution of equation (20) can be obtained as following

$$(\Delta\varepsilon^{k+1}, d^{k+1}) = argmin_{\Delta\varepsilon, d} \frac{1}{2} \|J\Delta\varepsilon - m\|^2 + \alpha \|d\|_1 + \frac{\beta}{2} \left\| d - \Delta\varepsilon - b_d^k \right\|^2 \tag{21}$$

$$b_d^{k+1} = b_d^k + \Delta\varepsilon^{k+1} - d^{k+1} \tag{22}$$

Then minimizing equation (21) and (22) can be achieved by minimizing $\Delta\varepsilon$ and d separately as following [22-24]:

- $\Delta\varepsilon^{k+1} = argmin_{\Delta\varepsilon} \frac{1}{2} \|J\Delta\varepsilon - m\|^2 + \frac{\beta}{2} \left\| d - \Delta\varepsilon - b_d^k \right\|^2$
- $d^{k+1} = argmin_d \alpha \|d\|_1 + \frac{\beta}{2} \left\| d - \Delta\varepsilon^{k+1} - b_d^k \right\|^2$
- $b_d^{k+1} = b_d^k + \Delta\varepsilon^{k+1} - d^{k+1}$

3.2 Level Set method (nonlinear method)

Instead of finding the internal permittivity value $\mathcal{E}_{int}$ of an inclusion, the level set technique is capable of representing boundaries of different inclusions by the zero level set of a predefined "level set function" ψ which can be one or higher dimensional function. Through updating this level set function the reconstructed shapes can move accordingly towards to correct shape. For

a 2-dimentional problem, suppose D is the inclusion of interest. Subsequently the boundary of the inclusion ∂D will be the interface between the two materials and is represented by the zero level set of the function ψ as

$$\boldsymbol{\partial D} = \{\boldsymbol{r}: \ \boldsymbol{\psi}(\boldsymbol{r}) = \boldsymbol{0}\} \tag{23}$$

Therefore, the permittivity at each point, $\varepsilon\ (r)$ can be represented in terms of the level set function as

$$\boldsymbol{\varepsilon}\ (\boldsymbol{r}) = \begin{cases} \boldsymbol{\mathcal{E}_{int}\ for}\ \{\boldsymbol{r}: \ \boldsymbol{\psi}(\boldsymbol{r}) < \boldsymbol{0}\} \\ \boldsymbol{\mathcal{E}_{ext}\ for}\ \{\boldsymbol{r}: \ \boldsymbol{\psi}(\boldsymbol{r}) > \boldsymbol{0}\} \end{cases} \tag{24}$$

Consequently, the capacitance data can be defined as a function of the level set function $C = F\ (\psi(\varepsilon\ (r)))$.

At the first iteration, the level set function ψ is given as *a priori* assumption and in later iterations it is updated in such a way that reduces a given cost function in order to move the boundaries towards the correct solution. The initial guess of ψ can be any kind of function, though the distance function $\psi^k = -dist(\partial D)$ is commonly used. A circular inclusion was chosen to be the initial guess for the level set function. Different optimization techniques can be used in order to find the updates of the level set function ψ. A modified optimization approach based on the gauss-newton method was selected to derive the updates of ψ by minimizing the following objective functional $g(\varepsilon)$

$$arg\ \min_{\boldsymbol{\psi}} \boldsymbol{g}(\boldsymbol{\psi}) = \|\boldsymbol{F}(\boldsymbol{\psi}(\boldsymbol{\varepsilon}\ (\boldsymbol{r}))) - \boldsymbol{C}\|_{\boldsymbol{2}}^{\boldsymbol{2}} + \ \boldsymbol{\gamma Reg}(\boldsymbol{\psi}(\boldsymbol{\varepsilon}\ (\boldsymbol{r})) \tag{25}$$

The argument in the above generalized equation can be fixed according to the requirements of the solution. γ >0 is the regularization parameter, which can be tuned using different mathematical techniques and $Reg(\psi(\varepsilon\ (r))$ is the regularization term, which is an arbitrary functional that can take different forms depending on the regularization method applied [25-27]. A good advantage of the level set method is that the regularization term does not have much effect on the problem, which makes it better posed. By using a modified gauss-newton approach for minimizing $g(\psi)$in (25)**(25),** the following equation is derived for the level set evolution:

$$\boldsymbol{\psi}\ (\boldsymbol{\varepsilon})^{\boldsymbol{k+1}} = \boldsymbol{\psi}\ (\boldsymbol{\varepsilon})^{\boldsymbol{k}} + \boldsymbol{\xi}^{\boldsymbol{k}}(\boldsymbol{B}^{\boldsymbol{T},\boldsymbol{k}}\boldsymbol{B}^{\boldsymbol{k}} + \gamma^{\boldsymbol{k}}\boldsymbol{L}^{\boldsymbol{T}}\boldsymbol{L})^{-\boldsymbol{1}}\boldsymbol{B}^{\boldsymbol{T},\boldsymbol{k}}(\boldsymbol{F}(\boldsymbol{\psi}\ (\boldsymbol{\varepsilon})^{\boldsymbol{k}}) - \boldsymbol{C}) \tag{26}$$

With $B = SK$ and $K = c\chi$

In (26), ξ is the step size parameter which is the magnitude of change in shape per iteration. In this paper both ξ and γ were chosen empirically and were held constant for all iterations. B is the narrowband Jacobian matrix of only those few elements adjoining ∂D. Here S is the sensitivity matrix for all the elements of the FEM mesh. K is the discretised form of $\varepsilon = \varphi\ (\psi(r))$, which comprises the indicator function χ of a small narrowband of half width an FEM element centred at ∂D and a normalization constant c. Lastly, L is the regularization matrix, in this case $L^T L = I$ is used.

4 EXPERIMENTAL RESULTS

Figure 4 illustrates a typical ECT system, which consists mainly of three subsystems; the capacitance sensor, data acquisition unit and computer unit. Our capacitance measurement unit is PTL300E, which is a commercial product from process tomography LTD [28]. The signal frequency of the measurement system is 1.25 MHz, i.e., the period of switching is 0.8μs. This means that it provides enough time for the conductor to reach the electrostatic equilibrium [20]. The effective range of capacitance measurement is from 0.1 ff to 2.0 pf. The sensor consists of 12 electrodes. Figure 5 shows the cross-section of the 12-electrode ECT sensor used in our

experiment. The internal radius of the tank is R1=9.5cm the external is R2=10cm. Each electrode in the width of 4.5cm is evenly distributed on the periphery.

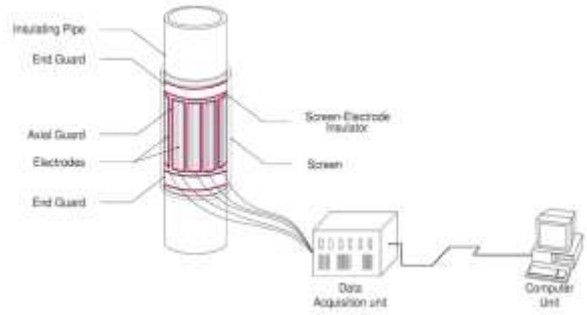

Figure 4. A typical ECT system

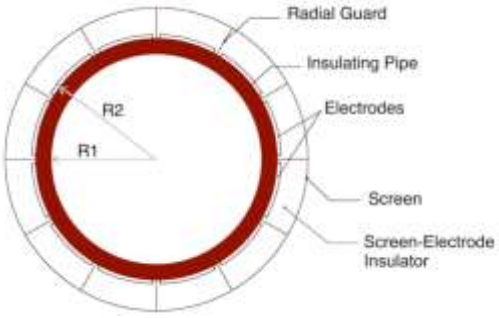

Figure 5. A cross-sectional view of the 12-electrode ECT sensor

Two types of sample are used in this experiment: sample 1 is a rectangular metal of size 8.2cm x7.5cm while sample 2 is a circular pipe with an external diameter of 6.3cm. In test 1 and 2 the rectangular metal is placed in the centre while in test 3, 4 and 5, one then two then three pipes are used respectevly. The proposed TV and LS algorithms are applied to reconstruct the images and the results are shown in Figure 6 along with the traditional Tikhonov regularization image reconstruction.

Test	Real distribution	Tikhonov	TV	Level set
1		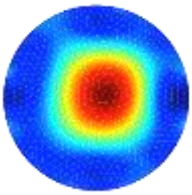	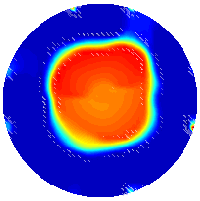	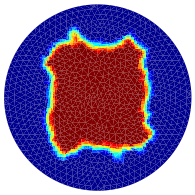
2		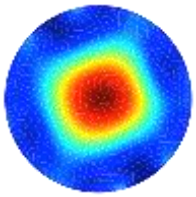	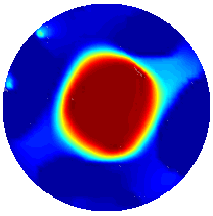	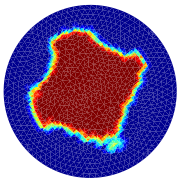
3		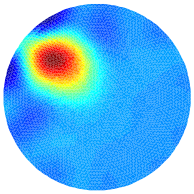	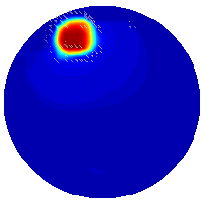	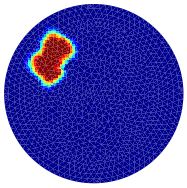
4		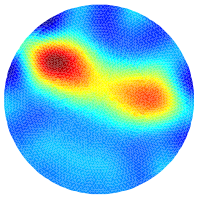	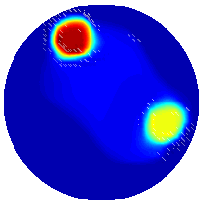	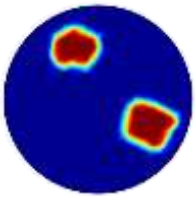
5		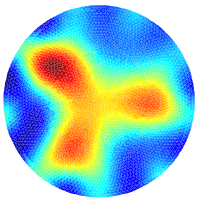	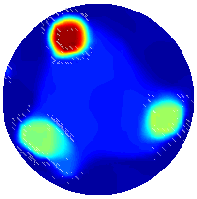	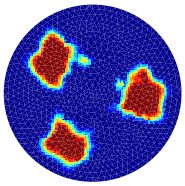
	(a)	(b)	(c)	(d)

Figure 6. Reconstructed images: (a) the experimental setup, (b) the reconstructed shape using the standard Tikhonov regularization method, (c) the reconstructed shape using Linear Total Variation method, (d) the reconstructed shape using Level Set method.

The level set algorithm is nonlinear algorithm and in every iteration the Jacobian matrix is recalculated. Although the linear methods are working fine the updating sensitivity maps will make the reconstruction near to the reality of the fact that the inversion is highly nonlinear here. The sensitivity with metallic sample included shows an expected area of zero sensitivity within the metal sample, and higher value of the capacitance changes due to short circuit effect of the space taken by metal and hence larger capacitance values.

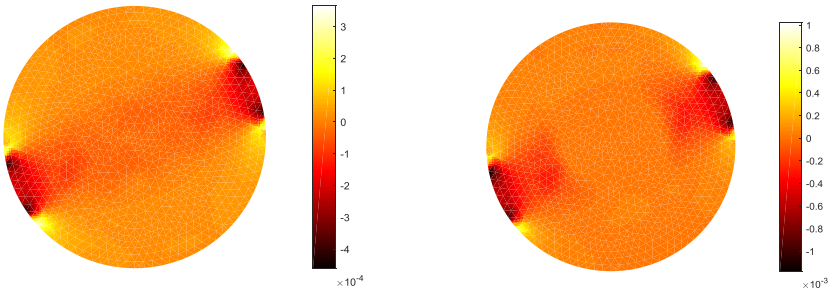

Figure 7. Sensitivity map for two opposite electrodes, left: free space, right: metal sample of figure 6.2 included in forward model.

5 DISCUSSIONS

The objective of this study is to demonstrate the possibility to adopt conventional ECT systems to image conductive materials such as metal. Initially the ECT forward model was verified, concluding a very large permittivity can be used to represent the metallic samples. From Figure 6, it can be seen that this objective can be better achieved by the level set method using the suggested metallic forward model based on high permittivity, which preserves the edges of images better than the TV or Tikhonov regularization methods. In terms of resolving different objects within the reconstructed images, LS method also was the most effective, although TV showed good results too compared to the traditional Tikhonov regularization method. Regularization parameter of 1e-5 was selected for all Tikhonov results, all three parameters in Bregman method was chosen to be 1 and number of iterations to 10, and in level set method the number of iterations was 12 and regularization parameter 1e-5. Tikhonov results depend directly on the choice of regularization parameter, while both TV and LS method are more robust against these parameters. Although LS method depends on the choice of permittivity values for the background and inclusion, this is not a problem for metallic sample imaging as any high permittivity value will be a good representation of metallic samples (e.g 4 or above). The computational time for a single step Tikhonov algorithm is 1.1 sec, while iterative TV has computational time of 2.1 sec for 10 iterations and nonlinear level set method took 5.3 sec for 12 nonlinear iterations. These are all done in a mesh of 2064 elements. The computational time is indicated for comparison purpose, for real time imaging this can be optimised.

In the level set method, the high-contrast inclusions are incorporated explicitly in the level set model without them dominating the entire domain. This makes the level set method more suitable for high-contrast image reconstruction with sharp boundaries than traditional regularization-based methods, which have the limitation of over-smoothing the reconstructed image particularly when a high-contrast inclusion is present. Furthermore, LS method can recover the geometry of the unknown interface despite any previous knowledge except for the permittivity value of the metal, which can be any arbitrary high value. This can be seen from our choice of the initial guess (i.e a circle in the centre of the domain), which does not nearly represent the true shape. Still, an accurate image was retrieved even though the initial guess was far away from the true shape.

Another advantage of the suggested level set method is its ability to improve the computational cost and the condition number of the discrete inverse problem by reducing the number of unknowns compared to other traditional pixel based image reconstruction methods. This can

be observed from equation (26) where the inverse problem is solved by using a narrow-band method in which only the adjacent pixels are inverted. Furthermore, since the level set method requires only absolute ECT data without any reference data, it is considered more robust for real-life applications. Based on the proposed forward model there is an infinite large change in permittivity, which is a suitable scenario for a binary reconstruction such as level set. Also, since TV method showed promising results as well, perhaps curved based regularization could be investigated in future enabling better shape recovery in level set reconstruction.

6 CONCLUSIONS

In this paper, ECT was used for metallic sample imaging. Due to the electrostatic equilibrium of metallic materials within static electric field, the capacitance measurements are increased. The proposed HP model of the metal for the forward problem approximates the existence of metal and compensates for the measurements very well. Furthermore, the efficiency of non-iterative linear methods (i.e Tikhonov regularization), TV regularization with linear measurements and iterative nonlinear methods (i.e LS) for the image reconstruction is investigated. The results demonstrated that both TV and LS methods could be adapted to image conductive inclusions such as metal with good resolution. Nevertheless, the produced images using LS method could identify sharp interfaces and distinguish multiple metal objects better.
For the high-contrast inherence of the metal imaging in ECT, level-set algorithm has a very suitable application by binarizing the sensing region: set a single high value on the estimated region of metal inclusions and a single low value on the background area. Thus, it distinguishes multiple metallic objects clearly. For most ECT applications, the recovery of the shape of the inclusion is more important than the recovery of the permittivity values of the enclosed materials. For such applications, the Level set method can be employed successfully to produce good images. However, the time spent for iterative calculation is longer than a single-step algorithm, such as Tikhonov regularization.
The experimental results showed that ECT can image metal as the same as the dielectric samples. This indicates that the application of conventional ECT can be extended to metal samples, especially using level-set algorithms to find the boundary of the metal. The proposed algorithms shows great potential for imaging metal using conventional ECT system, however, they are open for enhancement and further development. For instance, the level set method can be used to image objects with more than two different conductivity or be used to image situations with non-closure interface. Also, since both LS and TV showed great potential for metal imaging using traditional ECT, TV can be incorporated in LS as regularization for further enhancement.

REFERENCES

[1] S. Huang, A. Plaskowski, C. Xie, and M. Beck, "Capacitance-based tomographic flow imaging system," *Electronics letters*, vol. 24, pp. 418-419, 1988.

[2] K. Brodowicz, L. Maryniak, and T. Dyakowski, "application of capacitance tomography for pneumatic conveying processes," *Tomographic techniques for process design and operation*, pp. 361-8, 1993.

[3] G. E. Fasching and N. S. Smith jr, "A capacitive system for three dimensional imaging of fluidized beds," *Review of scientific instruments*, vol. 62, pp. 2243-2251, 1991.

[4] S. Liu, W. Yang, H. Wang, F. Jiang, and Y. Su, "Investigation of square fluidized beds using capacitance tomography: preliminary results," *Measurement science and technology*, vol. 12, p. 1120, 2001.

[5] S. Wang, T. Dyakowski, C. Xie, R. Williams, and M. Beck, "Real time capacitance imaging of bubble formation at the distributor of a fluidized bed," *The chemical engineering journal and the biochemical engineering journal,* vol. 56, pp. 95-100, 1995.

[6] R. He, C. Beck, R. Waterfall, and M. Beck, "Applying capacitance tomography to combustion phenomena," In *proc. European concerted action on process tomography, Karlsruhe*, 1993, pp. 300-2.

[7] R. He, C. Beck, R. Waterfall, and M. Beck, "Finite element modelling and experimental study of combustion phenomena using capacitance measurement," *Process tomography—a strategy for industrial exploitation—1994,* pp. 367-76, 1994.

[8] R. C. Waterfall, R. He, N. B. White, and M. Beck, "Combustion imaging from electrical impedance measurements," *Measurement science and technology,* vol. 7, p. 369, 1996.

[9] R. B. White, "Using electrical capacitance tomography to monitor gas voids in a packed bed of solids," *Measurement science and technology,* vol. 13, p. 1842, 2002.

[10] O. Isaksen, A. Dico, and E. A. Hammer, "A capacitance-based tomography system for interface measurement in separation vessels," *Measurement science and technology,* vol. 5, p. 1262, 1994.

[11] Z. Huang, D. Xie, H. Zhang, and H. Li, "Gas–oil two-phase flow measurement using an electrical capacitance tomography system and a venturi meter," *flow measurement and instrumentation,* vol. 16, pp. 177-182, 2005.

[12] W. Yang, M. Adam, R. Watson, and M. Beck, "Monitoring water hammer by capacitance tomography," *Electronics letters,* vol. 32, pp. 1778-1779, 1996.

[13] W. Deabes and M. Abdelrahman, "Solution of the forward problem of electric capacitance tomography of conductive materials," In *the 13th world multi-conference on systemics, cybernetics and informatics: wmsci, orlando, florida, usa*, 2009.

[14] M. Zhang and M. Soleimani, "Imaging floating metals and dielectric objects using electrical capacitance tomography," *Measurement,* vol. 74, pp. 143-149, 2015.

[15] L. I. Rudin, S. Osher, and E. Fatemi, "Nonlinear total variation based noise removal algorithms," *Physica D: nonlinear phenomena,* vol. 60, pp. 259-268, 1992.

[16] S. Osher and J. A. Sethian, "Fronts propagating with curvature-dependent speed: algorithms based on hamilton-jacobi formulations," *Journal of computational physics,* vol. 79, pp. 12-49, 1988.

[17] F. Santosa, "A level-set approach for inverse problems involving obstacles," *Esaim: control, optimisation and calculus of variations,* vol. 1, pp. 17-33, 1996.

[18] M. E. Zakharia and P. Chevret, "A shape reconstruction method for electromagnetic tomography using adjoint fields and level sets," *inverse problems,* vol. Volume 16, pp. 1119--1156, 2000.

[19] A. Lefranc, "Reconstruction of a two-dimensional binary obstacle by controlled evolution of a level-set," *Inverse problems,* vol. 14, pp. 685-706, 1998.

[20] Z. Zushou, "The time to reach electrostatic equilibrium of a conductor," *Physics and engineering,* vol. 12, pp. 20-21, 2003.

[21] D. N. Dyck, D. A. Lowther, and E. M. Freeman, "A method of computing the sensitivity of electromagnetic quantities to changes in materials and sources," *IEEE transactions on magnetics,* vol. 30, pp. 3415-3418, sep 1994.

[22] J. F. Abascal, J. Chamorro-servent, J. Aguirre, S. Arridge, T. Correia, J. Ripoll, *et al.*, "Fluorescence diffuse optical tomography using the split bregman method," *Medical physics,* vol. 38, pp. 6275-84, 2011.

[23] T. Goldstein and S. Osher, "The split bregman method for l1-regularized problems," *SIAM journal on imaging sciences,* vol. 2, pp. 323-343, 2009.

[24] S. Osher, M. Burger, D. Goldfarb, J. Xu, and W. Yin, "an iterative regularization method for total variation-based image restoration," *Multiscale modeling & simulation,* vol. 4, pp. 460-489, 2005.
[25] N. Irishina, D. Álvarez, O. Dorn, and M. Moscoso, "Structural level set inversion for microwave breast screening," *Inverse problems,* vol. 26, no. 3, pp. 163-117, 2010.
[26] M. Soleimani, W. R. B. Lionheart, O. Dorn , "Level set reconstruction of conductivity and permittivity from boundary electrical measurements using experimental data," *Inverse problems in science & engineering,* vol. 14, pp. 193-210, 2006.
[27] L. A. Vese and T. F. Chan, "A multiphase level set framework for image segmentation using the mumford and shah model," *International journal of computer vision,* vol. 50, pp. 271-293, 2002.
[28] M. Byars. (5 may 2016). *Process tomography ltd electrical capacitance tomography system type PTL300E*. Available: http://www.tomography.com/pdf/ptl300e.pdf
[29] P. Montesinos, J. F. P. J. Abascal, L. Cussó, J. J. Vaquero, M. Desco, "Application of the compressed sensing technique to self-gated cardiac cine sequences in small animals",*Magn Reson Med.*, 72(2): 369–380, 2013
[30] J. Ye, H. Wang and W. Yang, "A sparsity reconstruction algorithm for electrical capacitance tomography based on modified Landweber Iteration", Meas Sci & Tech, vol. 25, no.11, 115402, 2014.